ISSN 0021-3640, JETP Letters, 2014, Vol. 100, No. 3, pp. 181–186. © Pleiades Publishing, Inc., 2014.
Original Russian Text © E.A. Korznikova, S.V. Dmitriev, 2014, published in Pis'ma v Zhurnal Eksperimental'noi i Teoreticheskoi Fiziki, 2014, Vol. 100, No. 3, pp. 201–206.

Effect of the Configuration of a Wrinklon on the Distributions of the Energy and Elastic Strain in a Graphene Nanoribbon

E. A. Korznikova[a] and S. V. Dmitriev[a, b]

[a] *Institute for Metals Superplasticity Problems, Russian Academy of Sciences, ul. Khalturina 39, Ufa, 450001 Russia*
e-mail: elena.a.korznikova@gmail.com

[b] *St. Petersburg State Polytechnic University, ul. Politekhnicheskaya 29, St. Petersburg, 195251 Russia*

Received May 21, 2014; in final form, July 4, 2014

The formation of wrinkles in thin membranes is a widespread phenomenon. In particular, wrinkles can appear in graphene, which is the thinnest natural membrane, and affect its properties. A region where wrinkles with different wavelengths are linked is called wrinklon. Conditions of the fixing of an elastically deformed graphene sheet dictate a certain wavelength of wrinkles near the fixed edge. Wrinkles with a longer wavelength become more energetically favorable with an increase in the distance from the edge. As a result, wrinklons appear and reduce the potential energy of the system by uniting wrinkles into larger wrinkles with an increase in the distance from the edge. The possibility of implementing various equilibrium configurations of wrinklons at given plane strains in graphene has been demonstrated by the molecular quasistatic method. The distributions of the energy and elastic strain components in wrinklons with various configurations for nanoribbons with different widths have been calculated.

DOI: 10.1134/S0021364014150107

INTRODUCTION

Graphene is a new promising nanomaterial with unusual properties [1] having record stiffness under tension in the plane of a sheet [2], but a very small flexural stiffness. As a result, graphene tends to form wrinkles at the application of shear deformation [3–6] or compressing stresses in the plane of the sheet [7–9], under the action of thermal fluctuations or external force fields [10–12], owing to the interaction with a substrate [12–15], and at nanoindentation [16]. The formation of wrinkles is characteristic of many materials in the form of membranes or thin films, where a self-similar hierarchy of wrinkles appears under edge constraints [17]. This phenomenon is studied in many scientific fields, underlying the development of various technologies. In particular, it is known that the formation of wrinkles in thin metal films on a substrate can be used to create ordered structures [18].

The authors of [17] showed that the amplitude and wavelength of wrinkles in quite long membranes wavy fixed at the edges increase with the distance from a fixed edge. Transient regions where the wavelength of wrinkles changes are called wrinklons.

The authors of [15] showed that suspended graphene is more preferable than graphene on a substrate as a basic element for new-generation microelectronics. It was established that the formation of wrinkles significantly affects the properties of suspended graphene [19], stimulating great interest of experimentalists [11, 15] and theoreticians [4–6, 20–22] in study of the geometry of wrinkles and wrinklons.

The geometric properties of wrinkles in a graphene nanoribbon with fixed edges under uniform plane strain were analyzed recently in [4, 6, 14, 22]. The dependences of the wavelength, amplitude, and orientation of wrinkles on the components of uniform strain and width of the nanoribbon were determined. However, those works studied relatively narrow nanoribbons where the formation of wrinklons is energetically unfavorable. An increase in the width of the nanoribbon results in the appearance of the hierarchy of wrinkles with change in the wavelength of wrinkles in wrinklons.

In this work, a graphene nanoribbon with fixed edges and the width sufficiently large to form wrinkles with various wavelengths connected by wrinklons is studied with the focus on the energy of the transient region near the fixed edge of the graphene sheet.

DESCRIPTION OF THE MODEL

We perform calculations for a rectangular translation cell that contains four atoms and has the dimensions $a_0 = \sqrt{3}\,\rho_0$ and $b_0 = 3\rho_0$, where ρ_0 is the interatomic distance. Translation cells are specified by indices m and n. The (m, n) translation cell in Fig. 1 is shaded. The atoms in a translation cell is specified by the index $k = 1, ..., 4$. The x (y) coordinate axis corresponds to the zigzag (armchair) direction. The calculation cell had the dimensions of $M = 56, 64, 72, ...,$ 104 translation cells in the x direction and $N = 700$ cells in the y direction and contained $4 \times M \times N$ atoms. The

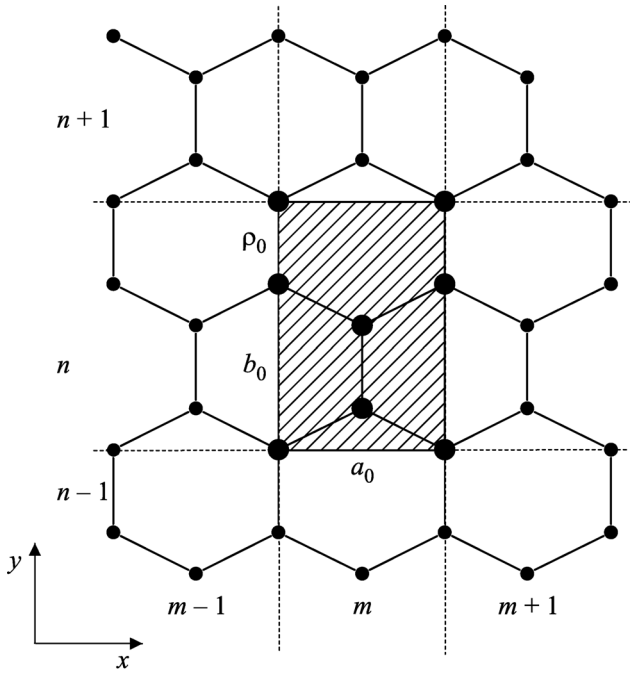

Fig. 1. Structure of undeformed graphene. The x (y) coordinate axis corresponds to the zigzag (armchair) direction. The length of an interatomic bond is ρ_0. A translation cell has the dimensions $a_0 = \sqrt{3}\,\rho_0$ and $b_0 = 3\rho_0$ and contains four carbon atoms. The cell with indices m and n is shaded.

uniform elastic strain of the graphene lattice was $\varepsilon_{xx}^0 = -0.08$ or -0.06 at fixed values $\varepsilon_{yy}^0 = 0.10$ and $\varepsilon_{xy}^0 = 0$. As a result, the dimensions of the translation cell became $a = a_0(1 + \varepsilon_{xx}^0)$ and $b = b_0(1 + \varepsilon_{yy}^0)$. The width and length of the deformed nanoribbon were $W = aM$ and $L = bN$, respectively.

Periodic boundary conditions were used for the edges parallel to the y axis. The displacements of atoms in the translation cells $n = 700$ were set to zero, simulating the fixed end of the nanoribbon. The condition mirror symmetry of atomic displacements with respect to the $(xz) = 0$ plane was imposed on the other end of the nanoribbon, which made it possible to consider only half of the nanoribbon with two fixed ends.

To describe the interatomic interactions, we used a standard set of molecular dynamics potentials [23], which provides the equilibrium length of a valence bond $\rho_0 = 1.418$ Å. The standard set of interatomic potentials was successfully tested in study of the heat conductivity of a graphene nanoribbon with rough edges [23], determination of the stability region of a graphene sheet uniformly deformed in its plane [24], determination of the geometric parameters of wrinkles in graphene nanoribbons with fixed edges [22], study of clusters of discrete breathers in deformed graphene [25], and study of discrete breathers at the edge of a graphene nanoribbon [26, 27].

Applied elastic strains induce a compressive membrane force T_x and tensile membrane force T_y so that unidirectional wrinkles are formed along the nanoribbon.

The relaxation dynamics of the nanoribbon under given initial conditions is studied in order to find its equilibrium configuration.

In this work, we study wrinklons, i.e., transient regions connecting wrinkles with different wavelengths. The initial conditions were specified so as to simulate a transition between wrinkles with different wavelengths in the graphene nanoribbon. To this end, the displacements of atoms in the direction normal to the plane of the nanoribbon were specified in the form of sinusoidal functions: $\Delta z(x, y) = A_1\sin(2\pi x/\lambda_1)$ in the interval $0 \le n \le 550$ and $\Delta z(x, y) = A_2\sin(2\pi x/\lambda_2)$ in the interval $551 \le n \le 699$, where λ_1 coincides with the width W of the nanoribbon, $\lambda_2 = \lambda_1/2$ or $\lambda_1/3$, and $A_1 = A_2 = 0.1$ Å are taken for the amplitudes of sinusoidal displacements. For such small amplitudes, interatomic bonds were not broken at the places of joining of waves with different λ values. The initial displacements in the plane of the graphene sheet and initial velocities of atoms were zero. Figures 2a and 2b show atoms of the nanoribbon having (gray) positive and (black) negative displacements in the direction normal to the plane of the nanoribbon obtained according to the initial conditions.

SIMULATION RESULTS

The relaxation of atoms in the structures shown in Figs. 2a and 2b results at $\varepsilon_{xx}^0 = -0.08$ in the formation of structures shown in Figs. 2c and 2d, respectively. Figure 2 also shows the dependences of (e) the potential energy e per atom and (f) the maximum displacement ΔZ of atoms from the plane of the nanoribbon on the number n after the relaxation of the nanoribbon for $\varepsilon_{xx}^0 = -0.08$ under the initial conditions (solid lines) $\lambda_1 \longrightarrow \lambda_1/2$ and (dotted lines) $\lambda_1 \longrightarrow \lambda_1/3$. It is noteworthy that $e(n) = (1/4M)\Sigma_{m=1}^{M}\Sigma_{k=1}^{4} e_{m,n,k}$, where $e_{m,n,k}$ is the potential energy of the (m, n, k) atom.

According to Fig. 2e, the dependences $e(n)$ for two resulting equilibrium configurations multiply intersect each other. In order to reveal which transient configuration has the lower total potential energy, we calculate the quantity $E = (4M/W)\Sigma_{n=0}^{N}[e(n) - e(0)]$. Here, $e(0)$ is the potential energy per atom in translation cells with $n = 0$ (far from the fixed edges of the nanoribbon). We calculated the energies of configurations obtained after relaxation under two initial conditions, $\lambda_1 \longrightarrow \lambda_1/2$ and $\lambda_1 \longrightarrow \lambda_1/3$, for nanoribbons with the elastic strain components $\varepsilon_{xx}^0 = -0.06$ and $\varepsilon_{yy}^0 = 0.10$ (see Fig. 2g), as well as $\varepsilon_{xx}^0 = -0.08$ and $\varepsilon_{yy}^0 = 0.10$

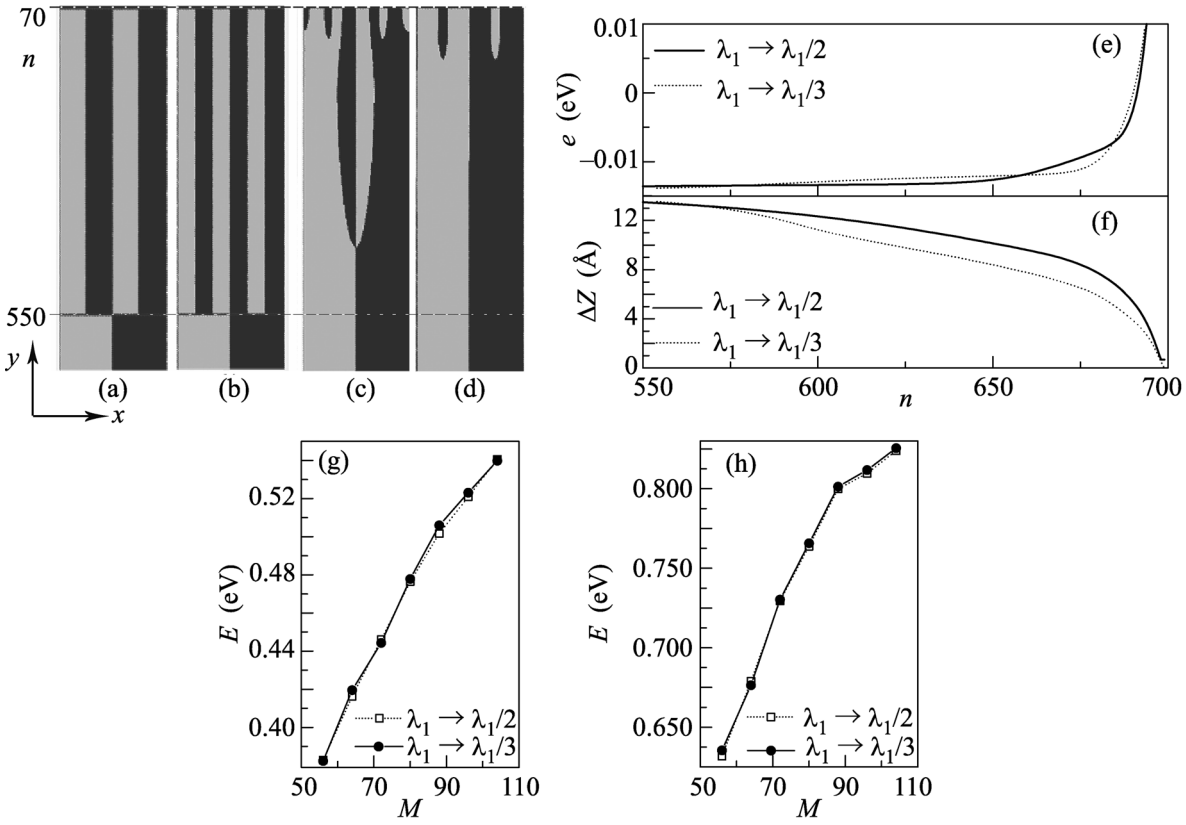

Fig. 2. (a, b) Fragment of the nanoribbon near the fixed edge under the initial conditions simulating the transition of a wrinkle with the wavelength $\lambda_1 = W$ to wrinkles with the wavelengths (a) $\lambda_1/2$ and (b) $\lambda_1/3$. Gray (black) color shows carbon atoms having positive (negative) displacements in the direction normal to the plane of the nanoribbon. (c, d) Same as in panels (a, b), but after relaxation to one of the minima of the potential energy of the nanoribbon at $\varepsilon^0_{xx} = -0.08$. (e) Potential energy per atom and (f) the maximum displacement of atoms from the (*xy*) versus the number *n* after relaxation for $\varepsilon^0_{xx} = -0.08$ under the initial conditions (solid lines) $\lambda_1 \longrightarrow \lambda_1/2$ and (dotted lines) $\lambda_1 \longrightarrow \lambda_1/3$. (g, h) Potential energy of the transient region near the fixed edge versus the width of the nanoribbon for the strain ε^0_{xx} = (g) –0.06 and (h) –0.08 under the initial conditions (open symbols) $\lambda_1 \longrightarrow \lambda_1/2$ and (closed symbols) $\lambda_1 \longrightarrow \lambda_1/3$.

(see Fig. 2h). It can be noted that, although the configurations of wrinklons, as well as the lengths of the transient region, are significantly different, the resulting energies of the transient regions almost coincide for the two strain values under consideration and for all wavelengths of wrinkles far from the edge. In particular, the energies of the transient regions for nanoribbons shown in Figs. 2c and 2d are $E_{\lambda_1 \to \lambda_1/2} = 0.82391$ eV/Å and $E_{\lambda_1 \to \lambda_1/3} = 0.82552$ eV/Å.

It also follows from Figs. 2g and 2h that the energy of the transient region far from the fixed edge increases slightly slower than linearly with the wavelength of wrinkles because the number of degrees of freedom for the reduction of the energy through the creation of transient regions with incommensurate transitions of the wavelength of wrinkles is larger for the longer edge of graphene.

The profiles of wrinklons appearing after relaxation are shown in Fig. 3 as the dependence of the displacement ΔZ of $k = 1$ atoms from the plane of the graphene sheet on the (*m*, *n*) translation cell under the initial conditions (a) $\lambda_1 \longrightarrow \lambda_1/2$ and (b) $\lambda_1 \longrightarrow \lambda_1/3$. The maximum ΔZ value is reached far from the fixed edge of the nanoribbon and is 1.4 nm for both cases, which corresponds to the equilibrium amplitude of the wrinkle with the wavelength λ_1 for the strains of graphene $\varepsilon^0_{xx} = -0.08$ and $\varepsilon^0_{yy} = 0.10$ [28]. The wrinklon in Fig. 3a near the fixed edge within the width *W* contains five sign-alternating waves, which corresponds to the scheme shown in Fig. 2c. Several bends of the dependence $\Delta Z(n)$, which do not lead to a change in sign, are seen near the fixed edge in Fig. 3b in addition to the main waves with change in the sign of the function $\Delta Z(n)$ (see Fig. 2d). Thus, according to change in the sign of the function $\Delta Z(n)$, two transitions $\lambda_1 \longrightarrow$

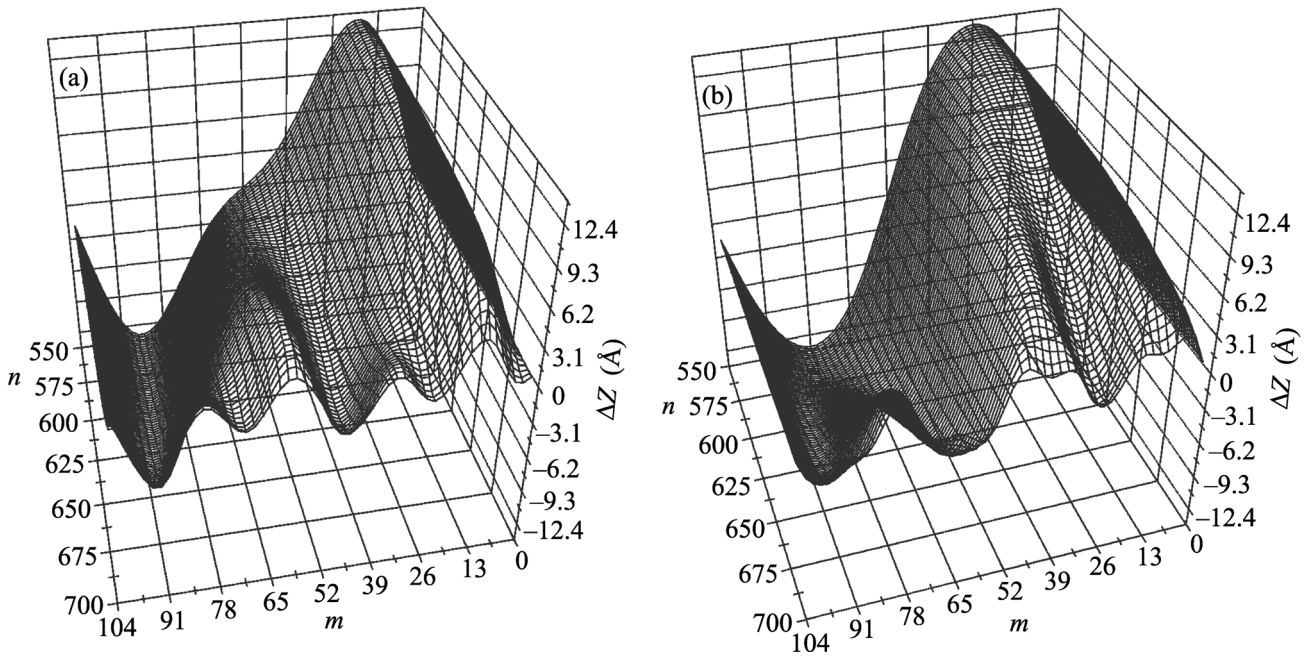

Fig. 3. Displacements ΔZ of atoms along the normal to the plane of the nanoribbon for equilibrium configurations obtained under the initial conditions (a) $\lambda_1 \longrightarrow \lambda_1/2$ and (b) $\lambda_1 \longrightarrow \lambda_1/3$ versus m and n for the plane strains $\varepsilon_{xx}^0 = -0.08$ and $\varepsilon_{yy}^0 = 0.10$.

$\lambda_1/2 \longrightarrow \lambda_1/5$ can be identified in Fig. 2c and one transition $\lambda_1 \longrightarrow \lambda_1/3$ is seen in Fig. 2d. However, in the latter case, as is seen in Fig. 3b, there are additional bends in $\Delta Z(n)$ near the fixed edge without change in the sign. The tendency of a decrease in the wavelength of wrinkles when approaching the fixed edge of the nanoribbon is clearly seen in both cases. This tendency was also observed experimentally in [12].

We consider elastic strains appearing in the nanoribbon after relaxation. Figure 4 shows the distributions of increases in elastic strains $\Delta\varepsilon_{xx} = \varepsilon_{xx} - \varepsilon_{xx}^0$ and $\Delta\varepsilon_{yy} = \varepsilon_{yy} - \varepsilon_{yy}^0$ near the fixed edge induced by the deviation of the graphene sheet from a planar shape at the formation of wrinkles and wrinklons. The x component of an increase in the elastic strain reaches $\Delta\varepsilon_{xx} = 0.03$ and is of the same order of magnitude as the strain $\varepsilon_{xx}^0 = -0.08$. No significant increase in $\Delta\varepsilon_{xx}$ is observed near the wrinklon. The component $\Delta\varepsilon_{yy}$ of an increase in the elastic strain is zero far from the fixed edge, increases slightly in the transient region, and is maximal (~0.003, which is an order of magnitude smaller than the strain $\varepsilon_{yy}^0 = -0.08$ in the plane of the graphene sheet) near the edge of the nanoribbon. The maximum $\Delta\varepsilon_{yy}$ value under the initial condition $\lambda_1 \longrightarrow \lambda_1/3$ is slightly smaller than that under the condition $\lambda_1 \longrightarrow \lambda_1/2$.

DISCUSSION AND CONCLUSIONS

It was previously shown experimentally [12] and through atomistic simulation [28] that the potential energy per atom in the case of unidirectional uniform wrinkles in the graphene nanoribbon depends on the wavelength as $e \sim \lambda^{-2}$. The wavelength of wrinkles near fixed edges is determined by the fixing conditions and the strain of graphene. An increase in the wavelength of wrinkles in wrinklons is energetically favorable with an increase in the distance from the fixed edge.

In this work, the molecular quasistatic simulation has shown that different initial conditions can result in different stable configurations of wrinklons with different energies. In particular, the configuration shown in Figs. 2c and 3a has a lower energy than that shown in Figs. 2d and 3b. Despite a significant difference in the length and configuration of the two resulting equilibrium structures, the difference in their energy is small. In the former and latter cases, $E_{\lambda_1 \to \lambda_1/2} = 0.82391$ eV/Å and $E_{\lambda_1 \to \lambda_1/3} = 0.82552$ eV/Å.

Perturbation introduced by the fixed edge to all characteristics under study (potential energy density e, amplitude ΔZ of displacements perpendicular to the plane of the nanoribbon, and components of an increase in the strain $\Delta\varepsilon_{xx}$ and $\Delta\varepsilon_{yy}$) propagates from the edge to the interior of the nanoribbon at a distance of no more than $3\lambda_1$.

We note that, although the configurations of wrinklons, as well as the lengths of the transient region,

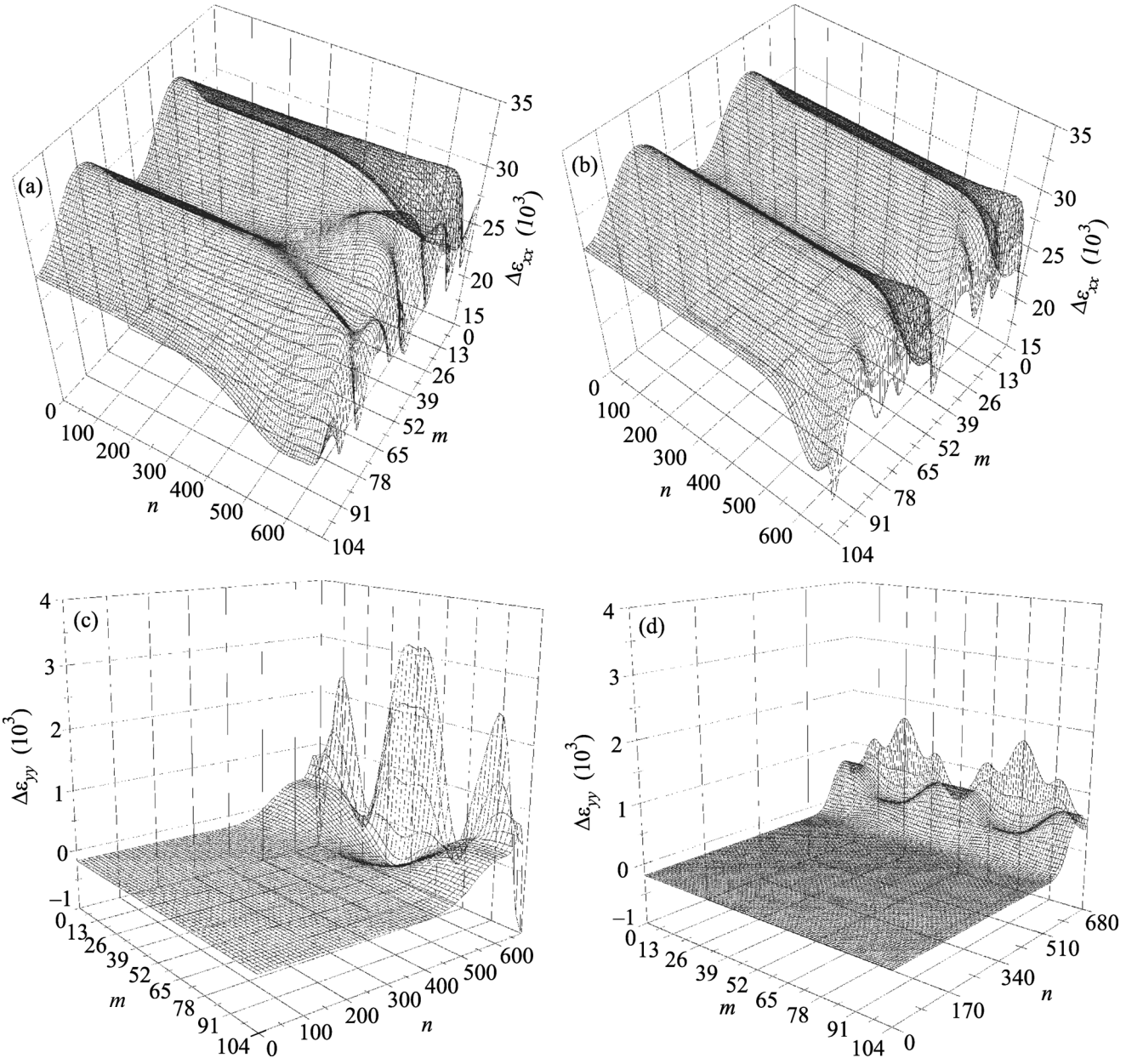

Fig. 4. Increases in elastic strains in the nanoribbon $\Delta\varepsilon_{xx} = \varepsilon_{xx} - \varepsilon_{xx}^0$ at (a) $\lambda_1 \longrightarrow \lambda_1/2$ and (b) $\lambda_1 \longrightarrow \lambda_1/3$ and $\Delta\varepsilon_{yy} = \Delta\varepsilon_{yy} - \varepsilon_{yy}^0$ at (c) $\lambda_1 \longrightarrow \lambda_1/2$ and (d) $\lambda_1 \longrightarrow \lambda_1/3$ versus m and n for the plane strains $\varepsilon_{xx}^0 = -0.08$ and $\varepsilon_{yy}^0 = 0.10$.

obtained at relaxation of the initial structures $\lambda_1 \longrightarrow \lambda_1/2$ and $\lambda_1 \longrightarrow \lambda_1/3$ are significantly different, the resulting energies of the transient regions almost coincide for the two strain values under consideration and for all wavelengths of wrinkles far from the edge. This apparently explains the variability of the shape of wrinkles experimentally observed in graphene.

The results obtained above can be useful for further investigations of the dependence of the physical and mechanical properties of graphene on the topology of wrinkles and wrinklons, which will promote the solution to the important technological problem of the control of the properties of graphene through its elastic strain.

The work of K.E.A. was supported by the Russian Foundation for Basic Research (project no. 14-02-97029-r povolzh'e-a). The work of S.V.D. was supported by the Russian Science Foundation (project no. 14-13-00982) and by the Ministry of Education and Science of the Russian Federation (program 5-100-2020).

REFERENCES

1. A. K. Geim and K. S. Novoselov, Nature Mater. **6**, 183 (2007).
2. J. U. Lee, D. Yoon, and H. Cheong, Nano Lett. **12**, 4444 (2012).
3. Z. Zhang, W. H. Duan, and C. M. Wang, Nanoscale **4**, 5077 (2012).
4. C. Wang, Y. Liu, L. Lan, and H. Tan, Nanoscale **5**, 4454 (2013).
5. K. Min and N. R. Aluru, Appl. Phys. Lett. **98**, 013113 (2011).
6. W. H. Duan, K. Gong, and Q. Wang, Carbon **49**, 3107 (2011).
7. A. H. Castro Neto, F. Guinea, N. M. R. Peres, K. S. Novoselov, and A. K. Geim, Rev. Mod. Phys. **81**, 109 (2009).
8. A. H. Castro Neto and K. Novoselov, Rep. Prog. Phys. **74**, 082501 (2011).
9. P. P. Azar, N. Nafari, and M. R. R. Tabar, Phys. Rev. B **83**, 165434 (2011).
10. A. Smolyanitsky and V. K. Tewary, Nanotechnology **24**, 055701 (2013).
11. W. Bao, K. Myhro, Z. Zhao, Z. Chen, W. Jang, L. Jing, F. Miao, H. Zhang, C. Dames, and C. N. Lau, Nano Lett. **12**, 5470 (2012).
12. L. Meng, Y. Su, D. Geng, G. Yu, Y. Liu, R. F. Dou, J. C. Nie, and L. He, Appl. Phys. Lett. **103**, 251610 (2013).
13. V. E. Calado, G. F. Schneider, A. M. M. G. Theulings, C. Dekker, and L. M. K. Vandersypen, Appl. Phys. Lett. **101**, 103116 (2012).
14. Z. Wang and M. Devel, Phys. Rev. B **83**, 125422 (2011).
15. W. Bao, F. Miao, Z. Chen, H. Zhang, W. Jang, C. Dames, and C. N. Lau, Nature Nanotechnol. **4**, 562 (2009).
16. A. J. Gil, S. Adhikari, F. Scarpa, and J. Bonet, J. Phys.: Condens. Matter **22**, 145301 (2010).
17. H. Vandeparre, M. Pieirua, F. Brau, B. Roman, J. Bico, C. Gay, W. Bao, C. N. Lau, P. M. Reis, and P. Damman, Phys. Rev. Lett. **106**, 224301 (2011).
18. Y. Mei, S. Kiravittaya, S. Harazim, and O. G. Schmidt, Mater. Sci. Eng. R **70**, 209 (2010).
19. V. M. Pereira, A. H. C. Neto, H. Y. Liang, and L. Mahadevan, Phys. Rev. Lett. **105**, 156603 (2010).
20. C. Wang, L. Lan, and H. Tan, Phys. Chem. Chem. Phys. **15**, 2764 (2013).
21. C. G. Wang, L. Lan, Y. P. Liu, H. F. Tan, and X. D. He, Int. J. Solid Struct. **50**, 1812 (2013).
22. J. A. Baimova, S. V. Dmitriev, K. Zhou, and A. V. Savin, Phys. Rev. B **86**, 035427 (2012).
23. A. V. Savin, Yu. S. Kivshar, and B. Hu, Phys. Rev. B **82**, 195422 (2010).
24. S. V. Dmitriev, Yu. A. Baimova, A. V. Savin, and Yu. S. Kivshar, JETP Lett. **93**, 571 (2011).
25. J. A. Baimova, S. V. Dmitriev, and K. Zhou, Europhys. Lett. **100**, 36005 (2012).
26. E. A. Korznikova, A. V. Savin, Yu. A. Baimova, S. V. Dmitriev, and R. R. Mulyukov, JETP Lett. **96**, 222 (2012).
27. E. A. Korznikova, J. A. Baimova, and S. V. Dmitriev, Europhys. Lett. **102**, 60004 (2013).
28. E. A. Korznikova, Fundam. Probl. Sovrem. Materialoved. **11** (1), 22 (2014).

Translated by R. Tyapaev